

Article

In Vitro Anti-Tubulin Activity on MCF10A Cell Line and In Silico Rigid/Semiflexible-Residues Docking, of Two Lignans from *Bursera Fagaroides* var. *Fagaroides*

Verónica Rodríguez-López ¹, César Millán-Pacheco ¹, Judith González-Christen ¹, Maricruz Anaya-Ruiz ² and Omar Aristeo Peña-Morán ^{3,*}

- ¹ Facultad de Farmacia, Universidad Autónoma del Estado de Morelos, Cuernavaca 62209, Mexico; veronica_rodriguez@uaem.mx (V.R.-L.); cmp@uaem.mx (C.M.-P.); judith.gonzalez@uaem.mx (J.G.-C.)
² Laboratorio de Biología Celular, Centro de Investigación Biomédica de Oriente, Instituto Mexicano del Seguro Social, Metepec 74360, Mexico; manaya19@yahoo.com.mx
³ División de Ciencias de la Salud, Universidad de Quintana Roo, Chetumal 77039, Mexico
* Correspondence: omar.moran@uqroo.edu.mx; Tel.: +52-983-8350300

Abstract: Podophyllotoxins are natural lignans with known cytotoxic activity on several cell lines. The structural basis for their actions is mainly by the aryltetralin-lignan skeleton. Authors have proposed a cytotoxic mechanism of podophyllotoxins through the topoisomerase-II inhibition activity; however, several studies have also suggested that podophyllotoxins can inhibit the microtubules polymerization. In this work, the two possible mechanisms of action of two previously isolated compounds from the stem bark of *Bursera fagaroides* var. *fagaroides*: acetylpodophyllotoxin (1) and 5'-desmethoxydeoxypodophyllotoxin (2), was analyzed. An in vitro anti-tubulin epifluorescence on the MCF10A cell line and enzymatic topoisomerase II assays were performed. The binding affinities of compounds 1 and 2 in the colchicine binding site of tubulin by using rigid- and semiflexible-residues were calculated and compared using in silico docking methods. The two lignans were active by the in vitro anti-tubulin assay but could not inhibit TOP2 activity. In the in silico analysis, the binding modes of compounds into both rigid- and semiflexible-residues of tubulin were predicted, and only for the semiflexible docking method, a linear correlation between the dissociation constant and IC₅₀ previously reported was found. Our results suggest that a simple semiflexible-residues modification in docking methods could provide an in vitro correlation when analyzing very structurally similar compounds.

Keywords: lignans; tubulin; semiflexible docking; MCF10A; podophyllotoxins



Citation: Rodríguez-López, V.; Millán-Pacheco, C.; González-Christen, J.; Anaya-Ruiz, M.; Peña-Morán, O.A. In Vitro Anti-Tubulin Activity on MCF10A Cell Line and In Silico Rigid/Semiflexible-Residues Docking, of Two Lignans from *Bursera Fagaroides* var. *Fagaroides*. *Molecules* **2021**, *26*, 6155. <https://doi.org/10.3390/molecules26206155>

Academic Editors: Mejdí Snoussi and Adel Kadri

Received: 16 September 2021

Accepted: 9 October 2021

Published: 12 October 2021

Publisher's Note: MDPI stays neutral with regard to jurisdictional claims in published maps and institutional affiliations.



Copyright: © 2021 by the authors. Licensee MDPI, Basel, Switzerland. This article is an open access article distributed under the terms and conditions of the Creative Commons Attribution (CC BY) license (<https://creativecommons.org/licenses/by/4.0/>).

1. Introduction

Lignans have been classified according to their chemical structure into eight classes: furan, furofuran, dibenzylbutane, dibenzylbutyrolactone, aryl-naphthalene, dibenzocyclooctadiene, dibenzylbutyrolactol, and aryltetralin. Lignans that are metabolized by mammalian gut microflora produce so-called enterolignans [1]. In the Barker publication in 2019, multiple works are reported about the isolation of lignans from plant species, among which are those of the families: Fabaceae, Lauraceae, which is a valuable source of more than 270 lignans and neolignans; in addition to the Mexican plants of the *Bursera* genus, all of them used in traditional medicine. The strategies for isolation and analysis have been varied, from in vitro and in vivo studies, to in silico studies. Traditionally the health benefits attributed to lignans include lowered risk of heart diseases, menopausal symptoms, osteoporosis, and breast cancer; however, some biological activities have been additionally reported: the anti-inflammatory activity in vitro for the inhibition of 15-lipoxygenase, phospholipases A2, cyclooxygenase 1 and 2 enzyme activities; pharmacokinetics and toxicity (ADMET) profiles to establish if these compounds are lead-like/drug-like compounds [2]; but also further investigations have highlighted the importance of lignan-rich

foods and their usefulness to the chronic illness prevention, certain types of cancers and cardiovascular disease, as well as anticarcinogenic, antioxidant, estrogenic, and antiestrogenic activities [3].

Podophyllotoxin (POD), an aryltetralin lignan, was isolated originally from the ethanolic extract of *Podophyllum peltatum*. In 1880 POD caused great expectation for cancer treatment, leading to the characterization of its structure, evaluation of its biological activity, and discovery of its mechanism of action through the inhibition of the tubulin polymerization, a consequent cell arrest in G₂/M phase and cell death, via necrosis or apoptosis [4,5]. However, despite its great biological potential, its use in clinics was truncated due to its high gastric toxicity and low selectivity [6,7]. Nevertheless, podophyllotoxin has been a pharmaceutically active ingredient in topical solutions and creams to treat the *Condylomata acuminatum* infections [8,9].

POD-type lignans are compounds derived from the shikimate pathway, particularly from a phenylpropanoid precursor [10]. Lignans are formed by linking two C₆C₃ units and linked by a β-β (8-8'). Aryltetralin-lignans are formed by a system of five rings (A, B, C, D, and E) ranging from the dioxol ring (A), the tetralin ring (B and C) to the γ-lactone ring (D), and an aromatic ring in C-7' with α configuration (Figure 1). Studies have shown that A and E rings are essential for their activity, and on the other hand, aromatization of ring C leads to loss of action [11].

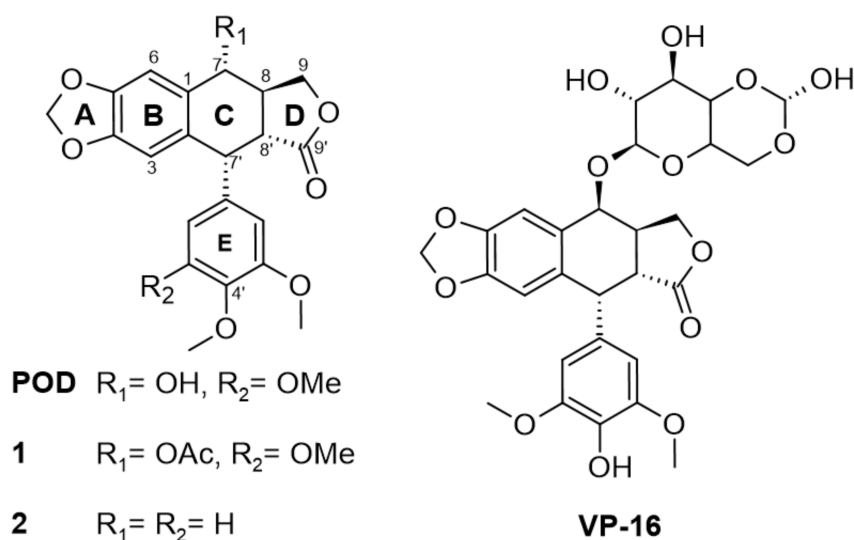


Figure 1. Modifications in structure between podophyllotoxin (POD) and etoposide (VP-16) and compounds 1 and 2.

In Figure 1, the chemical structures of lignan-type compounds used in this work are shown. For example, POD, 1, and 2 share the aryltetralin-type lignan structure, whose differences are found in C-7 and C-4', for POD a hydroxy (OH-) and a methoxy (OMe-) groups are found, for compound 1, an acetyl group (OAc-) and a methoxy (OMe-), and for compound 2 a hydrogen (H-) substituent in both positions can be found. On the other hand, VP-16 is classified as a semisynthetic epipodophyllotoxin with hydroxyl in C-4' and an acetylated glucose in the C-7 position.

POD mechanism of action is through a competitive inhibition in the colchicine binding site (named RB3-SLD by Ravelli and collaborators in 2004) [12], and is found among α and β tubulin subunits, and inserted between the strands S8 and S9, T7 loop, and the helices H7 and H8. Colchicine and POD also interact with the T5 loop of the α subunit; this interaction stabilizes the α/β-tubulin heterodimer. For microtubules stabilizations, longitudinal and lateral interactions between the tubulin molecules are required, where the M loops of the tubulin subunits play a central role in these interactions [12].

Etoposide (VP-16) is an epipodophyllotoxin that forms a ternary complex with DNA and topoisomerase II (TOP2) enzyme involved in DNA unwinding. VP-16 (Figure 1) prevents the DNA strands religation causing them to break, resulting in a premitotic block in the late S phase and early phase of G2 [6]. In contrast with POD, VP-16 incorporates demethylation in C-4' on E ring and an acetylated glucopyranoside in C-7 at C ring [13,14].

Some authors have proposed that the cytotoxic mechanism of POD derivatives is the inhibition of topoisomerase II [15–17]. However, several studies have also suggested inhibiting the microtubules polymerization as the cytotoxic mechanism of POD and its analogs [18–20].

This study aimed to explore the anti-tubulin effect on the MCF10A cell line (breast cell line), as well as the anti-TOP2 activity of two lignans previously isolated from *Bursera fagaroides* var. *fagaroides* [21], the compound 1 (acetylpodophyllotoxin) and the compound 2 (5'-desmethoxydeoxypodophyllotoxin) (Figure 1). In addition, the anti-tubulin compound POD, the TOP2-inhibitor anticancer drug VP-16, a lignan-based semisynthetic drug, and taxol (TAX) a microtubules-stabilizer compound [22], were also tested. Additionally, an in silico docking comparison method between rigid and semiflexible analysis in situ was performed with the crystalline structure model of tubulin heterodimer downloaded from Protein Data Bank [23] (code 1SA1). A correlation analysis was done with our previous reported cytotoxic evaluations [24] and the dissociation constant (K_D) calculated by the affinity energies acquired by the in silico docking methods.

2. Results

2.1. Microscopy Anti-Tubulin Test

Anti-tubulin effects of 1, 2, POD, VP-16, and TAX were evaluated by epifluorescence microscopy. Five micrographs were aleatory taken by sample, and each micrograph was measured by a pixel count analysis at the green channel (color of the fluorophore emission from AlexaFluor-488). In Figure 2 a representative micrograph for each treatment after 72 h of incubation is shown.

It is observed in Figure 2 that the control micrographs showed the conformation of the tubulin cytoskeleton (green), the nucleus (blue), the typical morphology of the MCF10A cells, and their average size. When the cells were treated with the VP-16, it showed microtubules with a low-grade nuclear fragmentation. However, it was also possible to observe cells that have not been modified in the tubulin cytoskeleton. Treated cells with POD presented a decrease in the cellular area and an alteration of the normal morphology. Treatment with TAX showed mostly normal nuclei; however, the signal corresponding to tubulin staining was increased (Figure 3), which could mean that the number of microtubules was also increased. Compounds 1 and 2 showed a decrease in the tubulin signal, but cells with standard size and morphology were also found compared with those of control.

The anti-tubulin activity was evaluated by micrographs analysis, showing that the vehicle did not affect tubulin stability (Figure 3). Each quantitation of relative tubulin content was normalized and compared with the control. When POD was tested, cells were observed with a low cellular area and a loss of normal morphology. The microtubules density percentage (MTD%) obtained was about $43.0\% \pm 8.6\%$, statistically different from the control ($100\% \pm 15.4\%$). Concerning VP-16, there was no statistical difference of MTD% that was about $88.0\% \pm 17.0\%$. Treatment with TAX resulted in a high signal of green staining belonging to tubulin stain ($137.3\% \pm 13.6\%$). A strong tubulin affinity characterizes TAX, and its action mechanism has been reported by promoting tubulin dimerization with stable microtubules formation that is not functional [26]. Compounds 1 and 2 presented a diminished tubulin signal, ($35.9\% \pm 9.0\%$ and $43.0\% \pm 13.0\%$, respectively).

To explore the counterpart of the mechanism of action reported by some research groups, the effect of compounds 1, 2, and positive controls (POD and VP-16) on the inhibition of the TOP2 enzyme was determined.

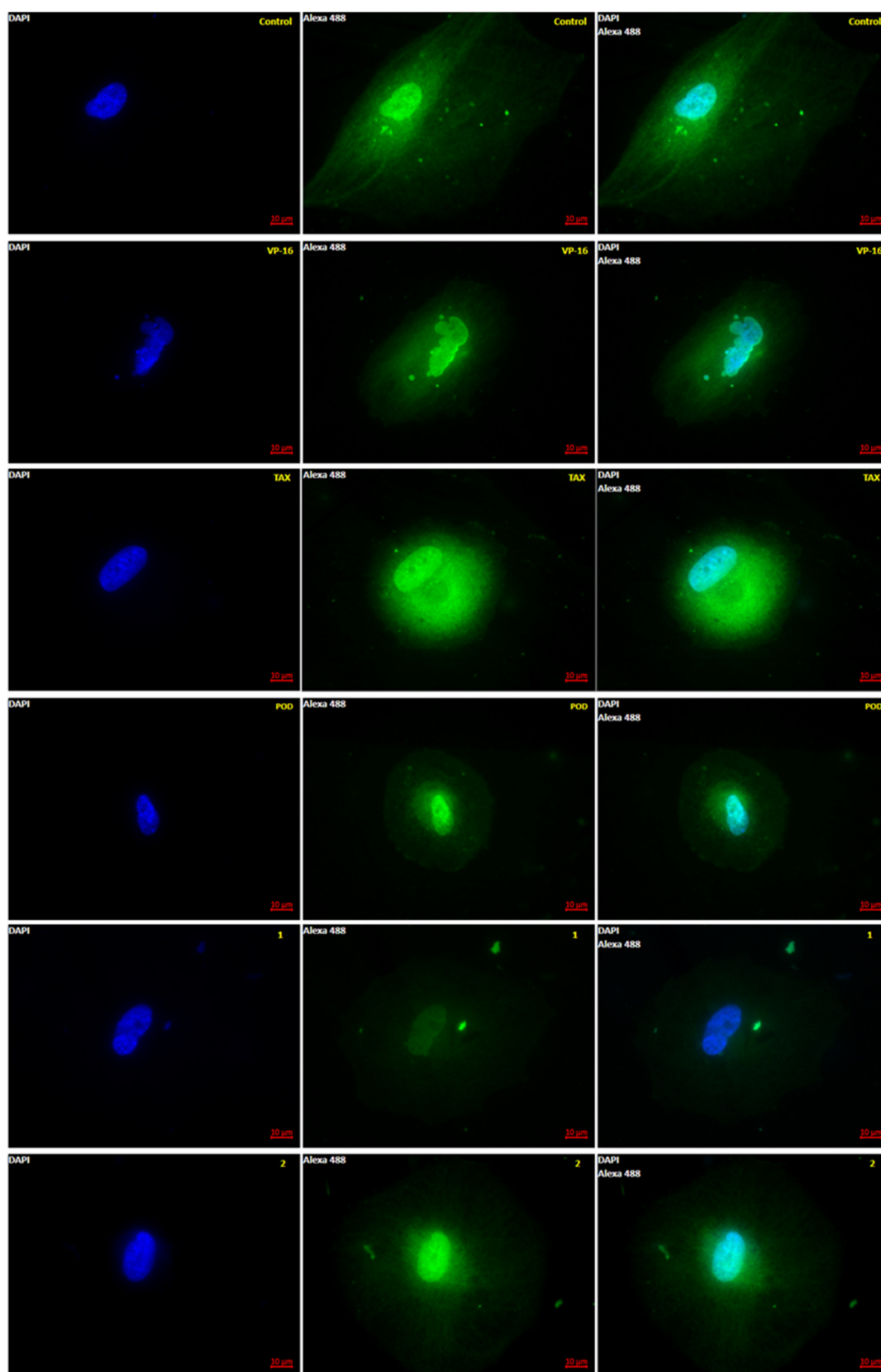


Figure 2. Microtubule polymerization dynamics observed by Epifluorescence. MCF10A cells were stained after 72 h of treatment with tubulin antibody (green) and DAPI (blue). Control was treated with DMSO (0.1%), and VP-16 (0.047 μM), TAX (0.002 μM) [25], POD (0.02 μM), compound 1 (0.318 μM), and compound 2 (0.092 μM). (Magnification 63×-oil).

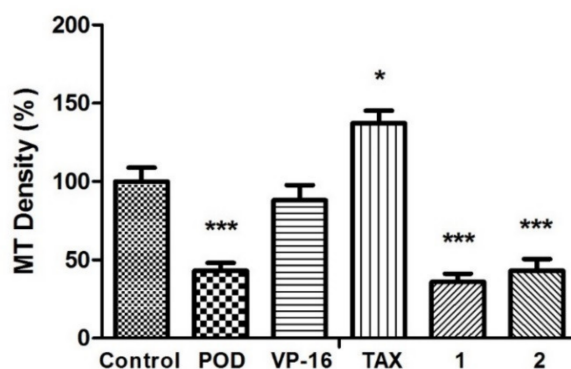


Figure 3. Microtubules densities quantification on MCF10A cells. N = 5 micrographs. Error bars indicate standard deviation (s.d.). Asterisks indicate statistical differences (One-way ANOVA and Dunnett Post-test) * $p < 0.05$, *** $p < 0.001$.

2.2. Topoisomerase II Inhibition Assay

TOP2 mode of action relaxes the supercoiled DNA and decatenates the kinetoplast DNA (kDNA). The VP-16 mechanism of action is over a DNA-TOP2-VP-16 complex formation. Results in the experiment in Figure 4 showed that VP-16 is interfering with the TOP2 action. However, compounds POD, 1, and 2 did not affect TOP2 decatenation properties.

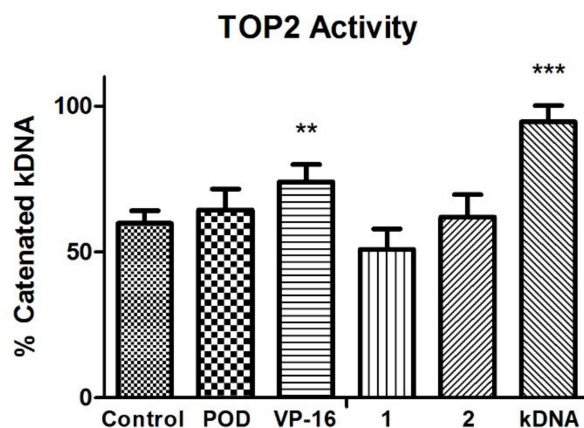


Figure 4. Topoisomerase II (TOP2) inhibition assay. Quantification of remnant kDNA after reaction incubation between TOP2- α and compound 1, 2, POD, and VP-16. Densitometric analysis of the agarose gel (n = 2 independent assays). Error bars indicated s.d., and asterisks indicated statistical differences (One-way ANOVA and Dunnett Post-test) ** $p < 0.01$, *** $p < 0.001$.

VP-16 showed decreased enzyme activity, unlike POD compounds 1 and 2, which offered a higher amount of decatenated kDNA. Those results suggested that compounds 1 and 2 have no inhibitory activity against TOP2, unlike VP-16. Additionally, the conformations of the compounds were analyzed with an *in silico* docking study, the results of which are shown below.

2.3. Rigid- and Semiflexible-Residues Molecular Docking

To further investigate the effect of inhibiting microtubules formation by compounds 1 and 2, the binding affinities energies between compounds and tubulin (into the colchicine binding site) were calculated. In addition, one bioinformatic analysis was performed for that purpose because no crystalline structure of tubulin from *Homo sapiens* in complex with POD was found in the PDB database. Therefore, an identity analysis between crystallized tubulin (gene name: TUBB2B) from *Bos taurus* (UniProt: Q6B856) and *Homo sapiens* (UniProt: Q9BVA1) was performed and showed 445 identical positions that represent a 100% of identity.

Based on the computational predictions, POD was inserted between the strands S8 and S9, T7 loop, and the helices H7 and H8. The binding affinity was about -8.6 ± 0.00 Kcal/mol; functional groups interactions with tubulin (rigid residues, Figure 5A) in the colchicine binding site were mainly by hydrophobic interactions between the E ring (trimethoxylated ring) and β Ala250, β Leu255, β Leu242, β Ile378, β Cys241, β Val318, and β Ala354, as well as van der Waals interactions were found with β Ala317, β Thr353. On the other hand, the residues α Val181, β Lys352, and β Asn350 interacted with the POD A ring (dioxol) mainly by electrostatics and hydrophobics (Figure 5B).

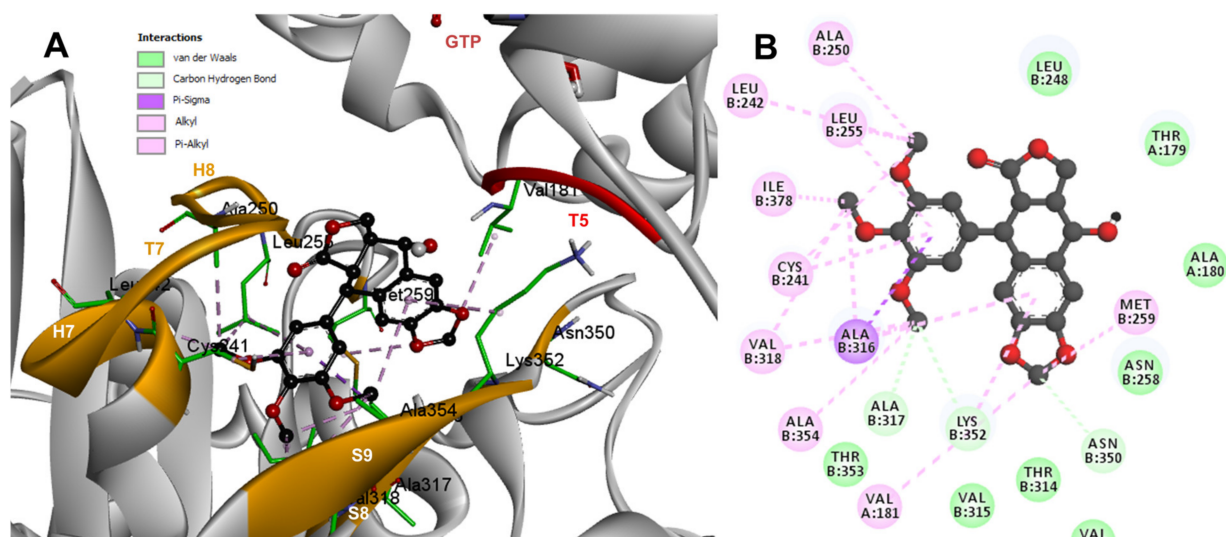


Figure 5. Interactions of POD with the α - and β -tubulin chains and rigid residues. (A) A displayed 3D diagram with the suggestive pose obtained by the most populated cluster selected for the conformation visualizations of POD. (B) 2D interaction diagram at the RB3-SLD site into tubulin heterodimer and POD. Interaction types between POD and the α - and β -tubulin dimer residues are shown in different colors (residues closer than 4\AA).

Conformations of compounds 1 and 2 were like POD, and both were inserted between the strands S8 and S9, T7 loop, and the helices H7 and H8 (Figures 6A and 7A) of the dimer of α - and β -tubulin computational model. The conformation interactions of compounds 1 and 2 showed tubulin-binding affinities of -6.9 ± 0.03 and -9.4 ± 0.00 Kcal/mol, respectively. Interactions between 1 and residues into the colchicine binding site were mainly by the E and A ring. The residues β Ala317, β Val238, β Lys352, β Ala354, β Val318, β Ile378, β Ala250, β Leu255, β Cys241, β Leu242, and β Ala316 were found interacting by hydrophobics with the E ring of compound 1, the residues β Lys352, β Asn350, β Met259, and α Val181 also interacted by hydrophobics to the A ring (Figure 6B). For compound 2, residues into the colchicine binding site were mainly by the E (dimethoxylated ring) and A ring. The residues β Lue248, β Val238, β Leu255, β Ala250, β Cys241, β Val318, β Ile378, β Ala354, β Ala316, were found interacting by hydrophobics with the E ring of compound 2, and residues β Ala316, β Val181, β Met259, β Lys252, β Asn350, β Val315 also interacted by hydrophobics but with the A ring (Figure 7B).

The conformations of suggestive poses were reported at the semiflexible residues docking analysis based on the computational predictions. POD was inserted between the strands S9, T7 loop, the helix H8 of the β -tubulin chain, and loop T5 of the α -tubulin chain (Figure 8A). The binding affinity was about -8.6 ± 1.15 Kcal/mol (remained, compared against the rigid docking); the interactions between POD functional groups and tubulin (semiflexible residues, Figure 8B) into the colchicine binding site were mainly by a hydrogen bond (POD as acceptor) formed by β Thr353 and the A ring (dioxol), as well as hydrophobic interactions between the E ring (trimethoxylated ring) and β Ala354, β Ala316, β Lys354,

and the methoxyl group of C-3'/C-5' (E ring could be rotating). The residue β Lys352 was found interacting by a Pi-alkyl type with B ring, and the residue β Thr353 formed another hydrogen bond (compound 1 as acceptor) with the A ring of compound 1 (Figure 9B). For compound 2, semiflexible residues into the colchicine binding site were mainly by the E (dimethoxylated ring). The residues β Lys352, β Leu248, and β Ala354 were found interacting by hydrophobics (Figure 10B).

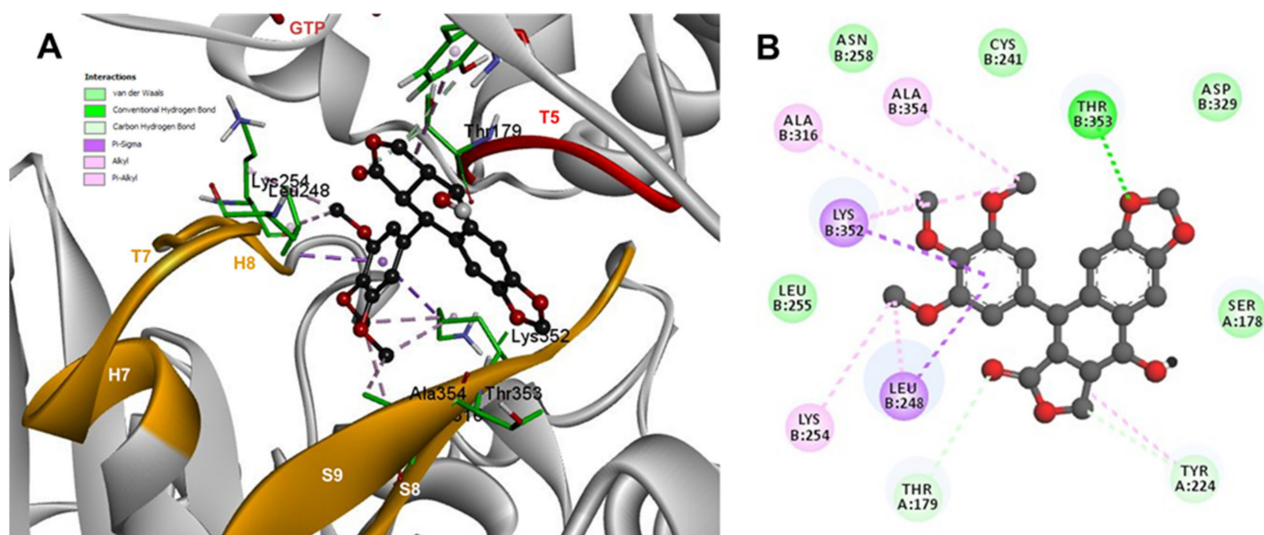


Figure 8. Interactions of POD with α - and β -tubulin chains and semiflexible residues. (A) A displayed 3D diagram with the suggestive pose obtained by the most populated cluster selected for the conformation visualizations of POD. (B) 2D interaction diagram at the RB3-SLD site into tubulin heterodimer and POD. Interaction types between POD and the α - and β -tubulin dimer residues are shown in different colors (residues closer than 4Å).

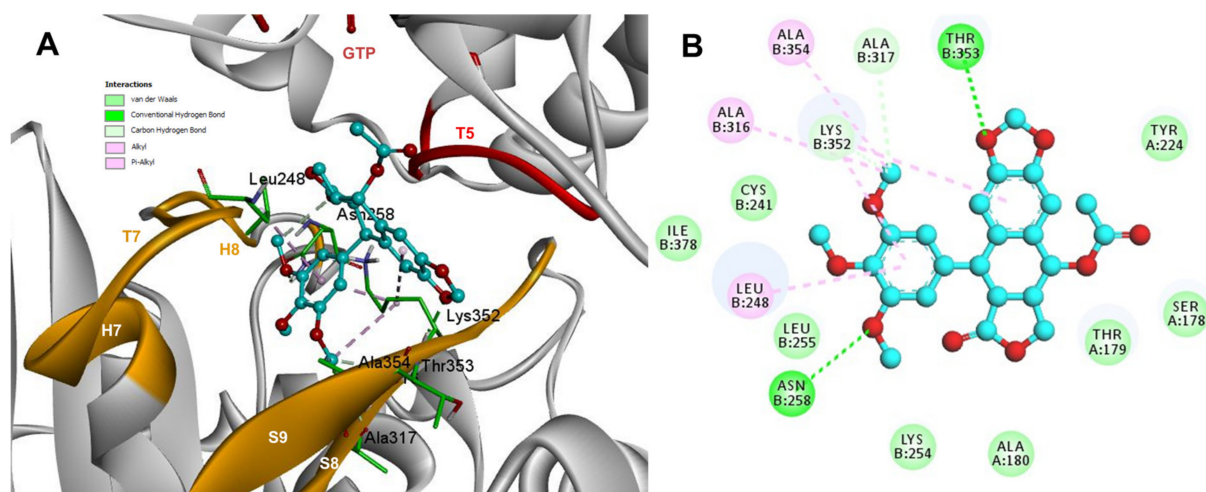


Figure 9. Interactions of 1 with α - and β -tubulin chains and semiflexible residues. (A) A displayed 3D diagram with the suggestive pose obtained by the most populated cluster selected for the conformation visualizations of 1. (B) 2D interaction diagram at the RB3-SLD site into tubulin heterodimer and 1. Interaction types between POD and the α - and β -tubulin dimer residues are shown in different colors (residues closer than 4Å).

The calculated affinity energies of POD compounds 1 and 2 in both rigid and semiflexible docking at the colchicine binding site within tubulin, are summarized in Table 1 along with the calculated dissociation constants (K_D) in molar concentrations. Linearity derived from this comparison is observed in Figure 7A for rigid residues docking and Figure 7B for semiflexible residues analysis. Results revealed a decrease in the affinity energy for

compound 1 compared to POD and compound 2 in both computational studies. Those results were correlated with the mean cytotoxic data obtained for the MCF10A cell line in previous studies (IC_{50} POD = 0.019 μ M, IC_{50} compound 1 = 0.318 μ M, and IC_{50} compound 2 = 0.092 μ M) [24]. The data shown in Table 1 suggested a better arrangement of the ligand structures at the RB3-SLD site due to the flexibility in the residues interacting with the POD in its crystallized format. In semiflexible docking, these residues may change their spatial form during the conformational docking search, as would occur in nature. Thus, our study has observed a better interpretation of what could happen between the assayed ligands and the inhibition of the tubulin polymerization. However, the affinity energy of binding has not improved compared to docking with rigid residues.

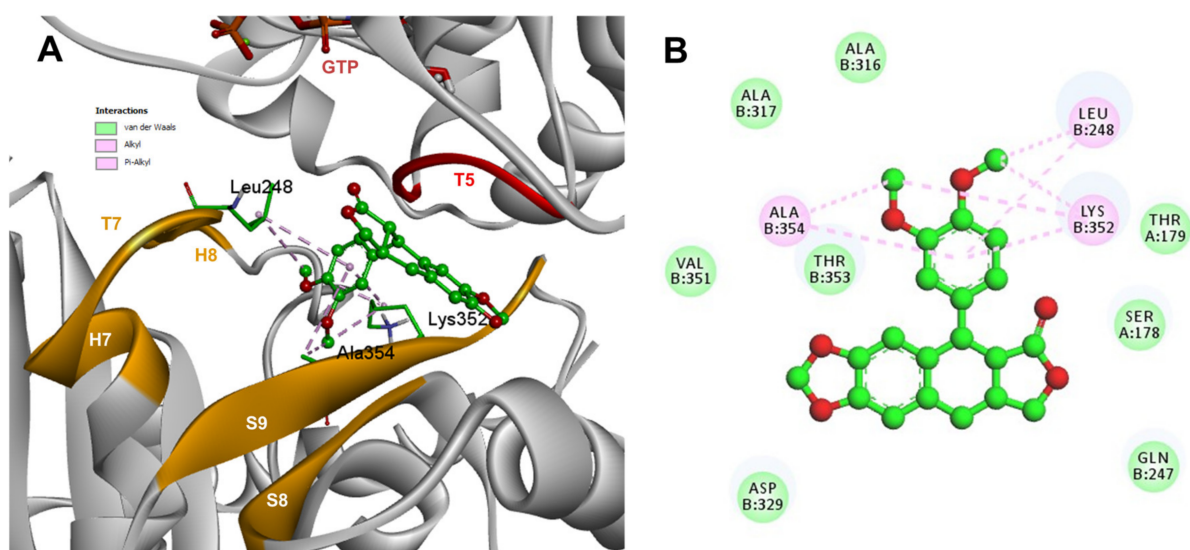


Figure 10. Interactions of 2 with α - and β -tubulin chains and semiflexible residues. (A) A displayed 3D diagram with the suggestive pose obtained by the most populated cluster selected for the conformation visualizations of 2. (B) 2D interaction diagram at the RB3-SLD site into tubulin heterodimer and 2. Interaction types between POD and the α - and β -tubulin dimer residues are shown in different colors (residues closer than 4Å).

Table 1. Tables display the mean affinity energy of binding (\pm s.d.) in addition to the mean calculated dissociation constant (K_D) from each ligand in the lowest energy cluster.

Compound	Rigid Residues		Flexible Residues	
	ΔG_b (Kcal/Mol)	K_D (M)	ΔG_b (Kcal/Mol)	K_D (M)
POD	-8.6 ± 0.00	$4.96 \times 10^{-7} \pm 0.00$	-8.6 ± 1.15	$1.44 \times 10^{-5} \pm 5.05 \times 10^{-5}$
1	-6.9 ± 0.03	$8.53 \times 10^{-6} \pm 5.08 \times 10^{-7}$	-3.6 ± 1.05	0.011 ± 0.03
2	-9.4 ± 0.00	$1.28 \times 10^{-7} \pm 0.00$	-10.8 ± 0.81	$3.10 \times 10^{-8} \pm 5.97 \times 10^{-8}$

In Figure 11, a linear relationship between in vitro activity and the proposed mechanism of action for evaluated compounds can be observed. In addition, a simple modified method for semiflexible-residues docking with Autodock vina made it possible to find a (slightly) better linear fit correlation between rigid residues ($R^2 = 0.926$, Figure 11A) and semiflexible residues ($R^2 = 0.944$, Figure 11B).

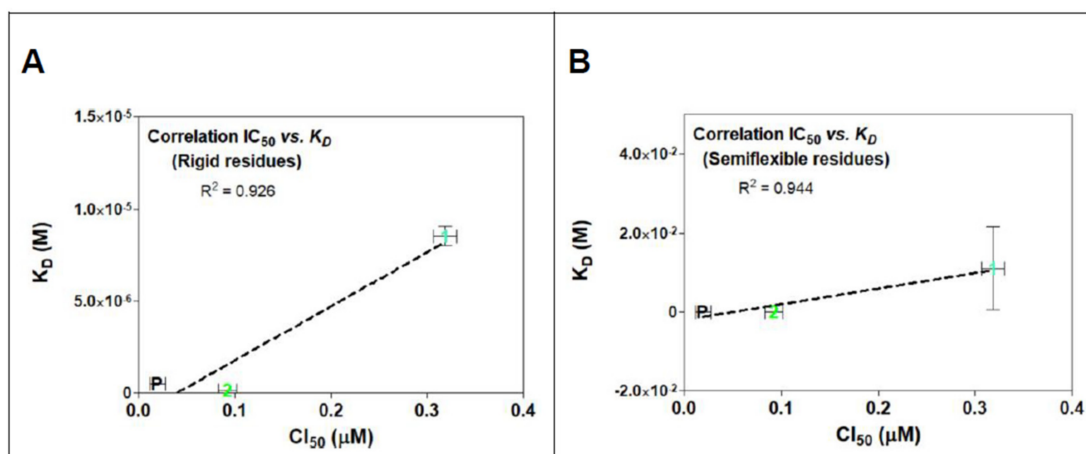


Figure 11. IC_{50} and K_D correlations analysis for rigid (A) and semiflexible (B) residues docking of compounds 1, 2, and POD on tubulin model 1SA1. Linearity is showed in both graphs between K_D and cytotoxic assay with MCF10A cells. There is also exposed the determination coefficient (R^2) from the linear regression analysis.

3. Discussion

MCF10A is a non-tumorigenic human mammary epithelial cell line employed in this study to explore the anti-tubulin effect of two lignans from *Bursera fagaroides* var. *fagaroides* and the correlations between in silico molecular docking either with rigid or semiflexible residues.

A low amount of quantitated tubulin in the anti-tubulin test probably suggested a destabilization of microtubule polymerized by POD, 1, and 2. Compounds affecting microtubule assembly lead to cell death or an aberrant mitosis exit [27]. Epifluorescence experiment against tubulin showed a changed morphology in cells when treated by 1 and 2, bringing a loss of cytoskeleton area. In addition, treated cells tended to round off. Some cells indicated a condensed and fragmented nucleus, suggesting that a low amount of semi-quantified tubulin could be produced by POD and compounds 1 and 2. Podophyllotoxin-type lignans are known to have cytotoxic activity [28–30], and could throw inhibition of the mitotic spindle by the binding with the α - and β -tubulin dimer. However, almost the same structure conformation (epipodophyllotoxins) is also known to be TOP2 inhibitors forming a TOP2-DNA-inhibitor complex [31,32].

Topoisomerase II (TOP2) mode of action relaxes the supercoiled DNA and decatenates the kinetoplast DNA (kDNA). On the other hand, the VP-16 mechanism of action is over a DNA-TOP2-VP-16 complex formation. The statistical analysis at the experiment in Figure 4 showed that VP-16 is interfering with the TOP2 action. However, compounds POD, 1, and 2 did not affect TOP2 decatenation properties.

In the in silico molecular docking analysis, energies calculated for compounds 1 and 2 did not differ considerably from those calculated for POD, suggesting that compounds 1 and 2 could dock to the RB3-SLD site by the same conformation as POD does, and some authors have described the structural basis of the cytotoxic effect of podophyllotoxins through the dioxolan tetralin lactone (A, B, C, and D rings) and the 3',4',5'-trimethoxyphenyl fragments [11,33].

The principal interactions of POD-type lignans with β -tubulin chain could be found with the A ring by electrostatics interactions between dioxolane ring oxygens and methylene type carbon with residues of β Asn258, β Lys352, and β Met259; and the methylene group between the two oxygen have presented VdW interactions with the β Val315. The B ring (aromatic C-H groups) have been reported mainly VdW-type interactions with β Met259 and β Lys352. The C ring (group HO-, for POD) has shown a polar interaction with the α Thr179 with the carbonyl group (not reproduced in this docking analysis). The D ring has been found to interact by VdW with the residues of β Leu248, β Lys254, and

β Leu255, and the trimethoxylated aromatic-type E-ring, have shown VdW interactions mainly with β Cys241, β Leu242, β Ala316, and β Ala317 (Figures 5–10).

The most advanced methods for computer-assisted drug design incorporate protein flexibility since these structures have natural movement, and a molecular docking analysis on a rigid protein could be missing some information about the binding between a ligand and a protein [34]. By configuring flexibility to residues in RB3-SLD, it was possible to analyze the changes (searching for better in vitro correlations) between the chemical conformations of each ligand and the binding affinity to tubulin heterodimer.

Comparison analysis between rigid and semiflexible docking allowed to find a linear correlation (Table 1), and by using semiflexible residues configurations, a determination coefficient of 0.944 was calculated, which suggested that although ligands could have some high structural similarities, and simple methods of semiflexible-residues molecular docking configurations could provide a piece of good correlative information with in vitro studies.

With the in silico analysis, the base for the inhibition of tubulin was understood in the colchicine binding site. Similar compounds could have similar mechanisms of action, but the potency of each compound depends on the stability in the binding site into the receptor. In the POD structure, the OH- group in the C ring at C-7 confers high strength to inhibit tubulin polymerization and thereby the capacity to prevent the tubulins heterodimers from passing from a curved structure to a straight one. The hydrogen bond between the C-7 in POD and α Thr179 could be fundamental to why affinity decreases when cells are treated by compounds 1 and 2. Our studies suggested an anti-tubulin but not anti-TOP2 bioactivity of acetylpodophyllotoxin (1) and 5'-desmethoxydeoxypodophyllotoxin (2) on cell line MCF10A.

However, why compounds 1 and 2 showed differences in their affinity for tubulin or cytotoxic potential remains uncertain since the structural differences are found minimal for compound 2 (lack of a methoxy in the E ring and one hydrogen atom at position C-7). Thus, there may be some other mechanism of action besides tubulin for this class of compounds, other than the inhibition of TOP2.

The mechanism of action proposed to 1, and 2 for the MCF10A cell line is correlated to the works of Antúnez-Mojica, et al., in 2016, for acetylphodophyllotoxin (1), in which a strong interaction with tubulin is reported vs. zebrafish, showing that the E ring is the main group for the interaction with the protein. On the other hand, 5'-desmethoxydeoxypodophyllotoxin (2) has the required structure to exert a favorable interaction to inhibit the mitotic spindle.

4. Materials and Methods

POD, VP-16, and TAX were purchased to Sigma-Aldrich (Sigma-Aldrich, Merck KGaA, Saint Louis, MO, USA). Rojas-Sepulveda, 2012 [21] isolated compounds 1 and 2. The MCF10A cell line (ATCC: CRL-10317) was purchased from the American Type Culture Collection (ATCC, Manassas, VA, USA) and cultured in MEGM medium (Lonza group, Basil, Switzerland) in a 5% CO₂ incubator at 37 °C. Cells were thawed according to the standard methods, and the experiments were performed using freshly thawed cells after three passages.

4.1. Microscopy Anti-Tubulin Test

The in vitro anti-tubulin test was performed with MCF10A cells. Briefly, cells (10⁴ cells/mL) were cultured in clean and sterile coverslips (1 cm²) inside of 12 wells flat-bottom cell culture plates and incubated in a controlled chamber (5% CO₂ and 37 °C) for eight hours. Afterward, cells were treated by the half inhibitory concentrations (IC₅₀) of POD, VP-16, 1, and 2, each of them calculated in previous work [24], TAX cytotoxic assay concentration (Sigma-Aldrich, Merck KGaA, Saint Louis, MO, USA) were taken by the work of Liebmann, 1996 [26]. Dimethyl sulfoxide (DMSO, Sigma-Aldrich, Merck KGaA, Saint Louis, MO, USA) (0.5%) was used as a control. After 72 h of treatment, cells were fixed with warm formaldehyde (4% in PBS) for 15 min, three times washed with

PBS, blocked by Bovine Serum Albumin (BSA) and triton X-100 (2.5% and 0.3% in PBS, respectively) for 60 min. Afterward, the antibody anti- α -tubulin-AlexaFluor 488 (Santa Cruz Biotechnology, Dallas, TX, USA) was added in a BSA solution (1% in PBS) and triton X-100 (0.3% in PBS) and incubated at 4 °C overnight. After incubation, cells were washed three times. Finally, a DAPI (Sigma-Aldrich, Merck KGaA, Saint Louis, MO, USA) solution was added (0.25 μ g/mL in PBS) to cells, incubated by 15 min, and washed three times with a PBS solution. Samples were visualized with a Zeiss Observer.Z1 microscope equipped with an AxioCam MRm camera and an Apotome illumination system with a 63x oil immersion objective.

4.2. Microtubules Semi-Quantitation

The microtubules semi-quantification was performed using the analyzer images program GIMP (v.2.8, GNOME Foundation, Orinda, CA, USA). The micrographs obtained from the nuclei and microtubule staining assays were processed. For each visualization, cells were selected manually with the selection tool of the software, and the histograms (in the green channel) were obtained for each cell selected. The percentage corresponding to the green pixels was taken from the histogram with the mean value of five analyzed images and plotted as the relative percentage microtubules density (MT density %), according to Formula (1):

$$\text{MT density (\%)} = A/B \times 100 \quad (1)$$

where A average pixels in the sample (anti-tubulin treated) and B average pixels in control (vehicle-treated).

The MT density (%) for each compound and control were graphed and compared against control with a t-test for unpaired data with a 95% confidence interval.

4.3. Topoisomerase II Inhibition Assay

This experiment was performed with a Topogen®kit (TopoGEN, Inc., Buena Vista, CO, USA) and the Topogen's pure TOP2 enzyme. The assay consisted of a reaction involving the triggering of DNA by the effect of TOP2; VP-16 was used as an inhibition control. Briefly, H₂O was added to make a final volume of 10 μ L, to which was added one μ L from buffer A and one μ L from buffer B (5X concentrated), one μ L from kDNA, 0.5 μ L of test compound (4 mg/mL), and 0.5 μ L of TOP2 enzyme (10 units/ μ L). The reaction was incubated in a heating plate for 45 min at 37 °C. Finally, two μ L of stop buffer were added. While incubation time was proceeding, a 1% agarose (Amresco, VWR Corporate Headquarters, Radnor, PA, USA) gel was prepared with ethidium bromide (EB, 0.5 μ g/mL; Sigma-Aldrich, Merck KGaA, Saint Louis, MO, USA), in which the samples were loaded after the incubation time, DNA was separated by electrophoresis at 100–150 V, with Tris, acetic acid, EDTA buffer (TAE), and photo-documented by an image analyzer Chemi doc MP (Bio-rad®). In addition, a linear DNA marker (Xho-I enzyme digestion), a decatenated DNA (DkDNA) marker (TOP2 activity), and a kDNA marker were added.

Quantification of remnant kDNA was obtained by densitometry according to Formula (2):

$$\text{Catenated kDNA (\%)} = A/B \times 100 \quad (2)$$

where A densitometry analysis in the sample. And B densitometry analysis in control (kDNA).

The Catenated kDNA (%) for each compound and controls (vehicle and kDNA) were graphed and compared with a t-test for unpaired data with a 95% confidence interval.

4.4. Flexible- and Rigid-Residues Molecular Docking

Compounds 1 and 2 were docked with the crystallographic heterodimer structure of tubulin from the Protein Data Bank (protein from *Bos taurus* but 100% identity with *Homo sapiens*), PDB code 1SA1, 4.2 Å of the resolution, and cocrystallized with guanosine-5'-diphosphate (GDP), guanosine-5'-triphosphate (GTP), a magnesium ion (Mg²⁺), and POD.

POD is found between the polar junction established between the α - and β -tubulin chains (colchicine binding site: RB3-SLD), and the complex has a curved conformation [12]. Amino acids interacting at 4 Å with POD are β Gly237, β Val238, β Thr239, β Thr240, β Cys241, β Leu242, β Leu248, β Ala250, β Asp251, β Leu252, β Lys254, β Leu255, β Asn258, β Met259, β Thr314, β Val315, β Ala316, β Ala317, β Val318, β Asn350, β Val351, β Lys352, β Thr353, β Ala354, and β Ile378 belonging to the β -tubulin chain and the amino acids of the α -tubulin chain α Thr179, and α Val181. For docking, semiflexible residues were configured using Autodock tools (v.1.5.6, Scripps Research Institute, La Jolla, CA, USA) and manually selected (Figure 12). Docking calculations (semiflexible and rigid configurations) were conducted with Autodock vina (v.1.1.2, Scripps Research Institute, La Jolla, CA, USA), and the grid was positioned at X = 115.9, Y = 90.1, Z = 4.3, with 15 Å by side dimensions, and 0.375 Å separated. Before docking experiments, the protocol was validated by docking the cocrystallized ligand (POD) and obtaining a Root Mean Square Deviation (RMSD) at the rigid of 2.487 Å and semiflexible of 2.480 Å.

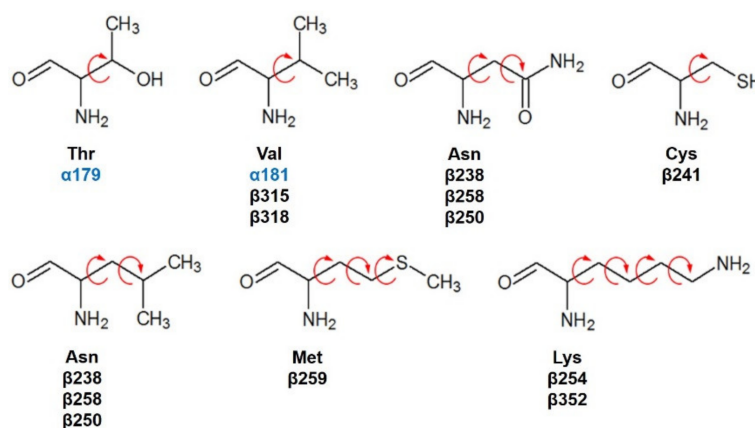


Figure 12. Semiflexible configured residues interacting with POD at 4 Å distance.

Ligands were optimized using an entire energy minimization force field (MMFF94) and docked with dihedral flexibility within the binding site RB3-SLD of the flexible-residues configured protein. For the protein, polar hydrogen atoms were added, and Kollman charges (AMBER) were assigned. Twenty-five independent runs for each ligand were performed. BIOVIA Discovery Studio (v3.5, Dassault Systèmes, Waltham, MA, USA) was used to visualize the final docked conformations for each ligand.

The most populated cluster was examined for rigid and semiflexible docking, and the mean of affinity energies was reported. In addition, the negatives affinity energy of binding was calculated as Kcal/mol, and the K_D of each compound was obtained through the Gibbs free energy and equilibrium equation.

4.5. Statistical Analysis

The statistical program GraphPad Prism (v.5.00, GraphPad Software, Inc., La Jolla, CA, USA) was employed to determine statistical differences in the experiments. For all statistical tests, significance was established at $p < 0.05$.

In Figure 13, a graphic scheme of the study approach is shown, and the flow of experiments and analysis of this work can be observed, which was carried out with two approaches: the in vitro approach focused on the determination of the possible mechanism of action of two isolated lignans of *Bursera fagaroides* var. *fagaroides* on a non-cancerous cell line; and the in silico approach, through a molecular docking analysis configured with both rigid and semiflexible residues, the results of which allowed obtaining a better linear correlation with the in vitro cytotoxicity data.

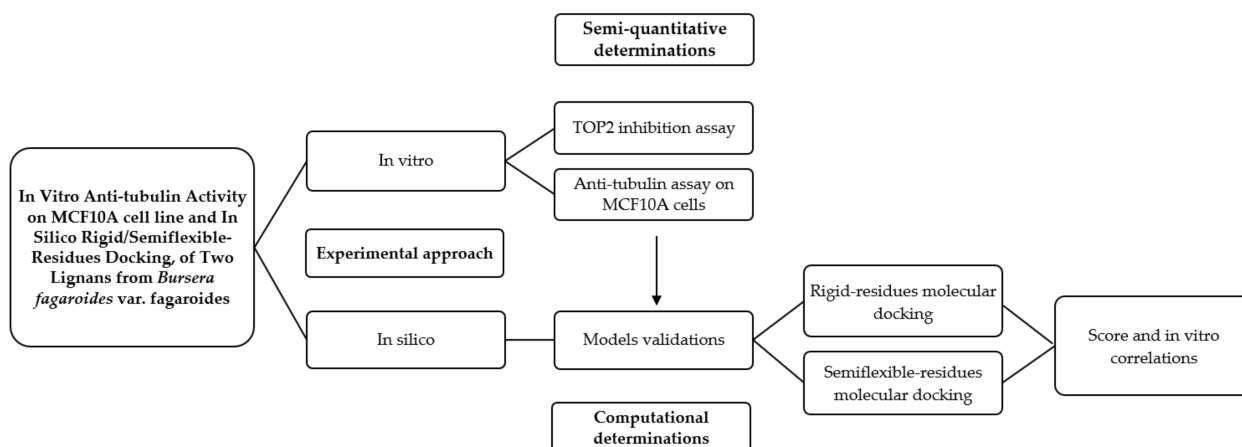


Figure 13. Graphical scheme of the study approach.

5. Conclusions

In conclusion, the treatment with lignans 1 and 2 forms *Bursera fagaroides* var. *fagaroides* showed less microtubule formation on MCF10A cells (first time reported). Therefore, Aryltetralin lignans are considered with great potential as POD analogs. However, they also share structural similarities with epipodophyllotoxins considered as TOP2 inhibitors. Our results have preliminarily demonstrated that compounds 1 and 2 do not form the TOP2-DNA-inhibitor complex. On the other hand, an in silico docking analysis between the tubulin dimer model configured with semiflexible residues allowed a good correlation between the cytotoxic effect and the ability to decrease the formation of microtubules in the MCF10A line. The favorable interactions within the colchicine binding site in tubulin, added to the microscopic effect observed in the microtubule staining assay, reinforce the hypothesis that podophyllotoxin-type lignans act as potent inhibitors of microtubule dynamics, forming the tubulin-aryltetralin lignan complex.

Author Contributions: Methodology: anti-tubulin assay, M.A.-R., and O.A.P.-M.; anti-TOP2 assay, J.G.-C., and O.A.P.-M.; in silico docking, C.M.-P. and O.A.P.-M.; resources, V.R.-L.; Formal analysis, all authors; writing—original draft preparation, O.A.P.-M. and V.R.-L.; writing—review and editing, all authors; funding acquisition, V.R.-L. and O.A.P.-M. All authors have read and agreed to the published version of the manuscript.

Funding: This research was funded by PROMEP-Redes.

Acknowledgments: The authors are thankful to Paola Maycotte González for technical support in epifluorescence micrographs visualizations and to Laura Álvarez for donating compounds 1 and 2 for this study.

Conflicts of Interest: The authors declare no conflict of interest.

Sample Availability: Samples of the compounds are not available from the authors.

References

1. Teponno, R.B.; Kusari, S.; Spitteller, M. Recent advances in research on lignans and neolignans. *Nat. Prod. Rep.* **2016**, *33*, 1044–1092. [[CrossRef](#)]
2. Barker, D. Lignans. *Molecules* **2019**, *24*, 1424. [[CrossRef](#)]
3. Durazzo, A.; Lucarini, M.; Camilli, E.; Marconi, S.; Gabrielli, P.; Lisciani, S.; Gambelli, L.; Aguzzi, A.; Novellino, E.; Santini, A.; et al. Dietary Lignans: Definition, Description and Research Trends in Databases Development. *Molecules* **2018**, *23*, 3251. [[CrossRef](#)] [[PubMed](#)]
4. Kamal, A.; Hussaini, S.M.; Malik, M.S. Recent developments towards podophyllotoxin congeners as potential apoptosis inducers. *Anticancer Agents Med. Chem.* **2015**, *15*, 565–574. [[CrossRef](#)]
5. Tseng, C.J.; Wang, Y.J.; Liang, Y.C.; Jeng, J.H.; Lee, W.S.; Lin, J.K.; Chen, C.H.; Liu, I.C.; Ho, Y.S. Microtubule damaging agents induce apoptosis in H.L. 60 cells and G2/M cell cycle arrest in H.T. 29 cells. *Toxicology* **2002**, *175*, 123–142. [[CrossRef](#)]
6. Canel, C.; Moraes, R.; Dayan, F.; Ferreira, D. Molecules of interest: Podophyllotoxin. *Phytochemistry* **2000**, *54*, 115–120. [[CrossRef](#)]

7. Xu, H.; Lv, M.; Tian, X. A review on hemisynthesis, biosynthesis, biological activities, mode of action, and structure-activity relationship of podophyllotoxins. *Curr. Med. Chem.* **2009**, *16*, 327–349. [[CrossRef](#)]
8. Longstaff, E.; VonKrogh, G. Condyloma eradication: Self-therapy with 0.15–0.5% podophyllotoxin versus 20–25% podophyllin preparations—An integrated safety assessment. *Regul. Toxicol. Pharmacol.* **2001**, *33*, 117–137. [[CrossRef](#)]
9. Peng, X.; Li, M. Medical Treatment of *Condyloma Acuminatum*, a Review on the Chemistry of Therapeutic Drugs. *J. Appl. Virol.* **2019**, *8*, 1–8. [[CrossRef](#)]
10. Dewick, P.M. *Medicinal Natural Products: A Biosynthetic Approach*, 3rd ed.; John Wiley & Sons: Chichester, UK, 2009; pp. 151–156.
11. Guerram, M.; Jiang, Z.-Z.; Zhang, L.-Y. Podophyllotoxin, a medicinal agent of plant origin: Past, present and future. *Chin. J. Nat. Med.* **2012**, *10*, 161–169. [[CrossRef](#)]
12. Ravelli, R.; Gigant, B.; Curmi, A.; Jourdain, I.; Lachkar, S.; Sobel, A.; Knossow, M. Insight into tubulin regulation from a complex with colchicines and a stathmin-like domain. *Nature* **2004**, *428*, 198–202. [[CrossRef](#)] [[PubMed](#)]
13. Montecucco, A.; Biamonti, G. Cellular response to etoposide treatment. *Cancer Lett.* **2007**, *252*, 9–18. [[CrossRef](#)] [[PubMed](#)]
14. Wu, C.C.; Li, T.K.; Farh, L.; Lin, L.Y.; Lin, T.S.; Yu, Y.J.; Yen, T.J.; Chiang, C.W.; Chan, N.L. Structural basis of type II topoisomerase inhibition by the anticancer drug etoposide. *Science* **2011**, *333*, 459–462. [[CrossRef](#)] [[PubMed](#)]
15. Thurston, L.S.; Irie, H.; Tani, S.; Han, F.S.; Liu, Z.C.; Cheng, Y.C.; Lee, K.H. Antitumor agents. 78. Inhibition of human DNA topoisomerase II by podophyllotoxin and alpha-peltatin analogs. *J. Med. Chem.* **1986**, *29*, 1547–1550. [[CrossRef](#)] [[PubMed](#)]
16. Hartmann, J.T.; Lipp, H.P. Camptothecin and podophyllotoxin derivatives: Inhibitors of topoisomerase I and II - mechanisms of action, pharmacokinetics and toxicity profile. *Drug Saf.* **2006**, *29*, 209–230. [[CrossRef](#)] [[PubMed](#)]
17. Liu, S.Y.; Hwang, B.D.; Haruna, M.; Imakura, Y.; Lee, K.H.; Cheng, Y.C. Podophyllotoxin analogs: Effects on DNA topoisomerase II, tubulin polymerization, human tumor KB cells, and their VP-16-resistant variants. *Mol. Pharmacol.* **1989**, *36*, 78–82.
18. Zhao, W.; Bai, J.K.; Li, H.M.; Chen, T.; Tang, Y.J. Tubulin structure-based drug design for the development of novel 4β-sulfur-substituted podophyllum tubulin inhibitors with anti-tumor activity. *Sci. Rep.* **2015**, *5*, 10172. [[CrossRef](#)] [[PubMed](#)]
19. Antúnez, M.M.; León, A.; Rojas-Sepúlveda, M.; Marquina, S.; Mendieta-Serrano, M.A.; Salas-Vidal, E.; Villarreal, M.L.; Alvarez, L. Aryldihydronaphthalene-type lignans from *Bursera fagaroides* var. *fagaroides* and their antimetabolic mechanism of action. *RSC Adv.* **2016**, *6*, 4950–4959. [[CrossRef](#)]
20. Desbène, S.; Giorgi-Renault, S. Drugs that inhibit tubulin polymerization: The particular case of podophyllotoxin and analogues. *Curr. Med. Chem. Anticancer Agents* **2002**, *2*, 71–90. [[CrossRef](#)]
21. Rojas-Sepúlveda, A.M.; Mendieta-Serrano, M.; Antúnez-Mojica, M.Y.; Salas-Vidal, E.; Marquina, S.; Villarreal, M.L.; Puebla, A.M.; Delgado, J.; Alvarez, L. Cytotoxic podophyllotoxin type-lignans from the steam bark of *Bursera fagaroides* var. *fagaroides*. *Molecules* **2012**, *17*, 9506–9519. [[CrossRef](#)]
22. Yang, C.H.; Horwitz, S.B. Taxol®: The first microtubule stabilizing agent. *Int. J. Mol. Sci.* **2017**, *18*, 1733. [[CrossRef](#)] [[PubMed](#)]
23. Berman, H.M.; Westbrook, J.; Feng, Z.; Gilliland, G.; Bhat, T.N.; Weissig, H.; Shindyalov, I.N.; Bourne, P.E. The Protein Data Bank. *Nucleic Acids Res.* **2000**, *28*, 235–242. [[CrossRef](#)]
24. Peña-Morán, O.A.; Villarreal, M.L.; Álvarez-Berber, L.; Meneses-Acosta, A.; Rodríguez-López, V. Cytotoxicity, Post-Treatment Recovery, and Selectivity Analysis of Naturally Occurring Podophyllotoxins from *Bursera fagaroides* var. *fagaroides* on Breast Cancer Cell Lines. *Molecules* **2016**, *21*, 1013. [[CrossRef](#)] [[PubMed](#)]
25. Liebmann, J.E.; Cook, J.A.; Lipschultz, C.; Teague, D.; Fisher, J.; Mitchell, J.B. Cytotoxic studies of paclitaxel (Taxol) in human tumour cell lines. *Br. J. Cancer* **1993**, *68*, 1104–1109. [[CrossRef](#)]
26. Steed, H.; Sawyer, M.B. Pharmacology, pharmacokinetics and pharmacogenomics of paclitaxel. *Pharmacogenomics* **2007**, *8*, 803–815. [[CrossRef](#)] [[PubMed](#)]
27. Mollinedo, F.; Gajate, C. Microtubules, microtubule-interfering agents and apoptosis. *Apoptosis* **2003**, *8*, 413–450. [[CrossRef](#)]
28. Kamal, A.; Ali-Hussaini, S.M.; Rahim, A.; Riyaz, S. Podophyllotoxin derivatives: A patent review (2012–2014). *Exp. Opin. Ther. Pat.* **2015**, *25*, 1025–1034. [[CrossRef](#)]
29. Lv, M.; Xu, H. Recent advances in semisynthesis, biosynthesis, biological activities, mode of action, and structure-activity relationship of podophyllotoxins: An update (2008–2010). *Mini Rev. Med. Chem.* **2011**, *11*, 901–909. [[CrossRef](#)]
30. Zhang, X.; Rakesh, K.P.; Shantharam, C.S.; Manukumar, H.M.; Asiri, A.M.; Marwani, H.M.; Qin, H.L. Podophyllotoxin derivatives as an excellent anticancer aspirant for future chemotherapy: A key current imminent needs. *Bioorg Med. Chem.* **2018**, *26*, 340–355. [[CrossRef](#)]
31. Hevener, K.; Verstak, T.A.; Lutat, K.E.; Riggsbee, D.L.; Mooney, J.W. Recent developments in topoisomerase-targeted cancer chemotherapy. *Acta Pharm. Sin. B* **2018**, *8*, 844–861. [[CrossRef](#)]
32. Zi, C.T.; Yang, L.; Xu, F.Q.; Dong, F.W.; Yang, D.; Li, Y.; Ding, Z.T.; Zhou, J.; Jiang, Z.H.; Hu, J.M. Synthesis and anticancer activity of dimeric podophyllotoxin derivatives. *Drug Des. Devel. Ther.* **2018**. [[CrossRef](#)] [[PubMed](#)]
33. Negia, A.S.; Gautam, Y.; Alam, S.; Chanda, D.; Luqman, D.; Sarkar, J.; Khan, F.; Konwar, R. Natural antitubulin agents: Importance of 3,4,5-trimethoxyphenyl fragment. *Bioorganic Med. Chem.* **2015**, *23*, 373–389. [[CrossRef](#)] [[PubMed](#)]
34. Carlson, H.A. Protein flexibility and drug design: How to hit a moving target. *Curr. Opin. Chem. Biol.* **2002**, *6*, 447–452. [[CrossRef](#)]